Eco-economic performance and application potential of a novel dual-source heat pump heating system

Yunhai Li[1], Yu Cui[1], Zhiying Song[2], Xudong Zhao[1, *], Jing Li[1, *], Chao Shen[3]

[1] Centre for Sustainable Energy Technologies, University of Hull, Cottingham Road, Hull, HU6 7RX, UK
[2] Department of Thermal Science and Energy Engineering, University of Science and Technology of China, Hefei 230026, China
[3] School of Architecture, Harbin Institute of Technology, Key Laboratory of Cold Region Urban and Rural Human Settlement Environment Science and Technology, Ministry of Industry and Information Technology, Harbin 150090, China
[*] Corresponding author. Tel.: +44-01482466684 (X. Zhao), +44-01482463611 (J. Li).
E-mail addresses: Xudong.zhao@hull.ac.uk (X. Zhao), Jing.li@hull.ac.uk (J. Li).

Abstract: Decarbonization of building heating is the key to carbon neutrality. Heat pumps have great potential to replace non-renewable heating devices, thus creating economic and renewable heating systems. To overcome the application challenges of conventional heat pumps (HP), a novel dual-source heat pump (DSHP) heating system and corresponding model are proposed in this paper. Simulated by the validated experiment-based model, the performance of the DSHP heating system is numerically investigated by comparing with different systems in various regions. The results show that the DSHP system has higher seasonal performance factors and near-zero defrosting costs when compared to the conventional HP heating system in different regions, resulting in 1.88%-21.53% reductions in annual heating bills and carbon emissions. Compared to the gas boiler heating system, the DSHP system can achieve 20.64%-54.36% of annual heating bill savings and 14.39%-86.09% of annual carbon reductions in selected regions. The investigation of heating characteristics and eco-economic performance of the DSHP system in different regions provided important guiding significance for the DSHP in global application, and thus contributes to achieving bill-saving and low-carbon heating and sustainable development.

Keywords: low-carbon heating, dual-source heat pump system, eco-economic performance, application potential

Nomenclature			
Symbols		D	DSHP
Q	Heat capacity (kW)	d	Defrosting
H	Heating amount (kWh)	e	Electricity
w	Power consumption (kW)	g	Gas
W	Energy consumption (kWh)	h	Heating
L	Heating load (kWh)	in	Indoor
t	Time spent (h)	m	Maximum
r	Defrosting time ratio (%)	out	Outdoor
T	Temperature (°C)	set	Setpoint
B	Heating bill (£)	***Abbreviations***	
C	Carbon emissions ($kgCO_{2e}$)	*COP*	Coefficient of performance
α	Energy price (£/kWh)	*SCOP*	Seasonal coefficient of performance
ε	Carbon emissions factor ($kgCO_{2e}$/kWh)	*SPF*	Seasonal performance factor
$\dot{m}$	Refrigerant mass flow rate (kg/s)	HP	Conventional heat pump
s	Entropy (kJ/kg/k)	GB	Gas boiler
Subscripts		MVHR	Mechanical ventilation heat recovery unit
A	System-A	DSHP	Double-source heat pump
B	System-B		
C	System-C		

1. Introduction

Carbon reduction is the top priority in to fight against climate change. Global energy structure is moving away from fossil fuel, shifting to renewable and eco-friendly energy. From 2010 onwards, the electricity share in final energy consumption has been increasing from 18% to 20% in 2018, while renewable proportion, such as solar, wind and biomass energy, raised from 20% to 25%. The 2050 roadmap of the International Energy Agency indicated that the energy transformation must accelerate, reaching 49% and 86% in electricity and renewable energy share in 2050, respectively [1]. Building energy consumption represents 46% of global final energy consumption. However, building heating, which is the greatest consumer of building energy, still highly relies on fossil energy, nowadays, contributing to 40% of global carbon emissions.

Building heating in the world is still ruled by fossil fuels. The stable heating performance and low energy prices of fossil fuels make gas boilers to be widely applied in the past century. At present, the growing development in carbon reduction, new energy policies and energy-efficient tendencies have accelerated the de-gas boiler process. Renewable heating devices, e.g., heat pumps, are increasingly popular among researchers and manufacturers led by governments. Net zero carbon building heating has tended to be the most essential technology for carbon neutrality. In the UK, the government came up with a series of plans to reduce carbon emissions and reach carbon net zero by 2050, which underlined the importance of building heating decarbonization and targeted installing 600,000 heat pumps a year by 2028 [2]. In China, the State Council recommended the cost-effective and renewable heat pump product for fossil boilers replacement in the Air Pollution Prevention and Control Action Plan, and the energy-saving production market subsidy scheme included the heat pump in the subsidy range with 10% of the retail price grant. The Chinese heat pump market will grow rapidly by over 200% in the next 5 years [3]. The European Commission signed up the REPowerEU plan in 2022 to set up an ambitious target in heat pump deployment, which aims to install 20 million heat pumps in 2026 and increase to 60 million in 2030, which will double the heat pump deployment speed [4].

In such a global policy environment, and as the share of renewable energy in the power sector has been increasing in recent years, air source heat pump (ASHP), as a kind of electricity-efficient device, is coming to be realized as the best alternative to gas boiler for heating decarbonization. However, compared with the traditional gas boiler (GB) heating system, the conventional ASHP heating system has obvious disadvantages obstructing its wide deployment.

(1) The heating capacity of the conventional ASHP heating system is severely impacted by the heat source temperature, dramatically decreasing as outdoor air temperature decreases, as does system efficiency [5]. Thus, the conventional ASHP heating system has poorer average efficiency and higher heating bill than that of the traditional GB heating system.

(2) The low water supply temperature of the conventional ASHP system requires a high cost of retrofitting in the heat terminals to increase the heating supply ability when substituting the traditional GB heating system. But, increasing the water supply temperature of conventional ASHP systems will result in large temperature differences between the heat source and the heat supply, leading to reduced heating capacity, increased power consumption and even destruction of the lifetime.

(3) The conventional ASHP system has severe frosting and defrosting problems that the traditional GB heating system does not. The outdoor heat exchanger of ASHP will form ice on the surface and defrost at the conditions of outdoor temperatures ranging from -7 ^{o}C to 5 ^{o}C, deteriorating the system efficiency and increasing heating bills [6].

Under the current global carbon-neutrality targets, there is an urgent need to address the obstacles to accelerate the adoption of heat pumps. A large number of investigations were conducted to optimize refrigerant circuits or introduce additional heat sources for better ASHP performance and wider deployment range.

Regarding the optimization of refrigerant circuits, most researchers proposed different multistage heat pumps to divide compression into several stages, which not only can effectively reduce the compression ratio of each stage for higher system efficiency but also prevent excessive compressor discharge temperatures at high water supply temperatures. Wang et al. [7] reported a novel double-stage coupled heat pump by cascading two different heat pumps. The testing results indicated that the novel heat pump worked more smoothly with an average coefficient of performance (COP) of 3.2 with a water supply temperature of 43 ^{o}C under outdoor temperatures between -6 ^{o}C to 6 ^{o}C, which increased the COP by 20% compared to the single-stage heat pump. Redon et al. [8] thermodynamically analysed the performance of vapor-injection two-stage heat pump systems by comparing them to a single-stage heat pump. They concluded that the vapor injection systems can provide heating capacity increments of 30% to 35% and COP improvements of 15% to 20%, finally achieving more than 30% seasonal COP increase under condensing temperature of 65 ^{o}C. Cheng et al. [9] numerically investigated a novel double internal auto-cascade two-stage compression heat pump system, which increased COP by 1.7%-4.4% compared to a vapor injection heat pump system under a condensing temperature of 50 ºC. Furtherly, Zou et al. [10] designed and optimized a cascaded vapor-injection heat pump system. The experiment and theoretical results showed that the novel triple stages heat pump had stable COPs between 1.16 to 1.58 when the outdoor temperature ranged from -10 ºC to 20 ºC under a high supply temperature of 140 ºC.

Apart from seeking breakthroughs from the refrigerant circuit, many researchers focused on the heat sources investigation, combining outdoor air with other heat sources to promote system stability as well as seasonal performance. Han et al. [11] experimentally investigated a multi-source coupled heat pump system, which can absorb heat energy from outdoor air and solar radiation by a novel collector/evaporator. The results indicated that the COP of the novel system was stable at 2.12 to 2.50 at outdoor temperatures of -16 ºC to -2 ºC and increased by 4.9% compared to the common HP system. Wang et al. [12] developed an innovative dual-source heating system with a novel heat pump and energy storage unit, which can obtain energy from the photovoltaic/thermal water exchanger and air heat exchanger to reduce heating cost by 45% and operate more stably when compared to an ASHP heating system. Jiang et al. [13] designed a triangular solar air collector-assisted air source heat pump, which had preheat, series and parallel modes to fully utilize the energy from solar radiation and air. The experiment results indicated the novel multi-source heat pump had a 64.4% higher average COP than the ASHP. Grossi et al. [14] tested a novel dual-source heat pump system with air and ground heat sources and compared it with an ASHP system by annual simulations, which indicated that the novel system reached 24.6% annual performance factor promotion and had more stable performance over the years. Fang et al. [15] considering the unstable of solar irradiation and outdoor air temperature, presented a novel ice source heat pump system with solar thermal panels and air heat exchangers. The experiment results showed that the novel system had less heating capacity fluctuation and a minimum COP of 3. Li et al. [16] analysed the characteristics of different heat sources and theoretically discussed the advantages of different hybrid source heat pumps. The results showed that hybrid heat sources heat pump systems had around 15% energy-saving rate when compared to single-source heat pump systems.

Investigations discussed above indicated that dual-stage and dual-source heat pump systems have a better ability to achieve high efficiency in low ambient temperatures and high water supply temperatures than conventional ASHP systems, effectively increasing the system stability in cold regions. However, they did not adequately consider frosting and defrosting influence on system performance deterioration. To solve the frosting problems, many researchers drew great attention to inventing effective frosting retarding and defrosting methods. The frosting retarding measures can be divided into active and passive forms. Active frosting retarding focuses on changing outdoor air conditions [17] and destroying frost [18], while passive frosting retarding focuses on the structure adjusting [19, 20] and surface coating for air heat exchangers [21]. The active forms have a deficiency that requires additional power consumption, and the passive forms need a high initial cost. As for defrosting methods, they are concluded into 5 different normal sorts, which are: (1) compressor shutdown defrosting, (2) electric heating defrosting, (3) hot water spraying defrosting, (4) hot gas bypass defrosting, and (5) reverse cycle defrosting. The first defrosting method can reduce the power consumption of defrosting at the cost of defrosting time, but only works when outdoor temperatures are higher than 1 ºC [6]. The electric heating and hot water spraying methods need high external power to achieve fast defrosting, which has very limited application. The widely applied hot gas bypass and reverse cycle methods are compressor-derived defrosting methods and have high power consumption.

Respecting the practical application, most buildings with traditional GB heating systems are not equipped with ventilation heat recovery devices due to the considerations of operation cost and system complexity at the beginning of construction, resulting in significant ventilation heat loss from exhaust air. Therefore, many low-carbon retrofit projects are replacing traditional GB heating systems by installing new systems with HPs and mechanical ventilation heat recovery units (MVHR). However, integrating HP and MVHR into low-carbon heating systems is not the optimal solution, as the complexity of the integrated system is much higher than that of the traditional GB system. Dodoo et al. [22] theoretically demonstrated that the impact of MVHR on building heating deeply relied on the type of heating system. Although MVHR can effectively reduce the heating load of buildings in cold weather, the additional ventilation power consumption could lead to higher energy bills compared to the traditional GB system.

The exhaust air of the building is a non-negligible heat source and the best option for frosting retarding and defrosting in the ASHP heating systems. Considering the problems of defrosting and ventilation heat recovery, building exhaust should provide more benefits than just ventilation. Therefore, Yi et al. [23] proposed and proved a concept of a novel dual-source heat pump, which can recover waste heat from building exhaust air with two-stage evaporation and vapor injection compression, and integrate a novel defrosting method by utilizing exhaust air for frosting retarding and defrosting. The results of their study indicated that the novel dual-source heat pump had better COP than the vapor injection heat pump and the ASHP, which can achieve a maximum COP of 3.65 at a water outlet temperature of 30 ºC and ambient temperature of 0 ºC. The previous works have proven the concept in low water outlet temperature range (<35 ºC). However, the system performance and characteristics at high water outlet temperatures have yet to be investigated.

To demonstrate the all-important high water outlet temperature performance and application potential, significant improvements have been made in the design of the system. In this paper, a dual-source heat pump (DSHP) prototype with compact construction and automatic control program, which is specially designed for high water outlet temperature and low ambient temperature application is presented and tested. Thereafter, a novel DSHP heating system for practical application with an innovative and simple structure is further proposed according to the manufactured prototype. Based on the experiment data, a building heating model of the novel DSHP heating system is developed and validated for investigations of its heating performance and application potential by comparing it to the conventional HP heating system and the traditional GB heating system. The characteristics and performances of the three different systems are compared to discover the advantages of the novel DSHP heating system. And then further eco-economic analyses are proposed according to the different regions with varying climatic conditions and energy policies, so the application of the novel DSHP heating system will be deeply studied and give out more instructional information for the DSHP deployment and achieving carbon neutrality targets.

2. Descriptions of the DSHP and corresponding heating system

2.1 Structure and experiment setup of the DSHP prototype

Figure 1 (a) illustrates the structure of the DSHP prototype, which has 2 low-pressure evaporators (LE), 1 medium-pressure evaporator (ME), 1 economizer, 1 plate-type condenser, 1 vapor injection compressor, 3 expansion valves and 5 air fans. It is seen that 2 exhaust air fans are installed on the top of the DSHP, and the other 3 discharger air fans are installed on the bottom. Figure 1 (b) shows the system diagram of the DSHP. From the side of the air-flowing direction, the exhaust air flows through the medium-pressure evaporator for the first-stage heat exchange. In this stage, the exhaust air will be cooled down by releasing a part of its heat energy into the medium-pressure refrigerant. At the same time, the outdoor air flows into the outdoor unit and mixes with the cooled exhaust air, becoming a warmer mixed air. The mixed air, thereafter, flows through the low-pressure evaporators for the second-stage heat exchange. In the second stage of heat recovery, the mixed air will release all the heat energy into the low-pressure refrigerant and becomes colder discharge air than the outdoor ambient. When it turns to the refrigerant side, analysing the refrigerant flow together with Figure 2, the vapor injection compressor extracts and compresses the evaporated refrigerant ($\dot{m}_1$) from the low-pressure evaporators (4'-5). and then mixed it with the medium-pressure refrigerant ($\dot{m}_2$) becoming a colder refrigerant mixture (4,5-6) before the second-stage compression. The refrigerant mixture ($\dot{m}_{\mathrm{tot}}$) after second-stage compression (6-1) will be discharged to the plate-type condenser, where the high-pressure refrigerant mixture ($\dot{m}_{\mathrm{tot}}$) will release a large amount of heat energy to the water (1-2). Subsequently, a part of the refrigerant flows into the medium-pressure evaporator ($\dot{m}_{2'}$) and economizer ($\dot{m}_{2''}$) for medium-pressure evaporation (3-4) after corresponding throttling. The rest refrigerant ($\dot{m}_1$) flows through the economizer for subcooling (2-2') followed by low-pressure evaporation (3'-4') in low-pressure evaporators, finishing a cycle. According to Figure 2, the energy flow and balance of DSHP can be formalized in Table 1. To sum up, the presented DSHP has the following extraordinary characteristics in conditions of cold weather and high water temperature:

(1) The waste heat of exhaust air is recovered in two-stage evaporation, forming double heat sources for the DSHP. And thus, the evaporation temperature difference of each stage is narrowed, and the evaporation temperatures ($T_{3'}$ and T_3) are promoted from the red dash lines (see Figure 2) to the black lines of 3-4 and 3'-4', respectively. So, the irreversible energy loss in evaporation is decreased and the compression ratios are reduced for each compression stage, leading to higher heating capacity (Q_{con}) and lower power consumption (W).

(2) The vapor injection compressor reduces the power consumption (W) and refrigerant discharge temperature (T_1) by dividing the compression process into two stages with medium vapor injection cooling. With the medium vapor injection cooling (4,5-6), the water outlet temperature can be raised, and the total refrigerant mass flow rate ($\dot{m}_{\mathrm{tot}}$) of the condenser is increased, as well as the heating capacity (Q_{con}).

(3) The warm exhaust air mixes with cold outdoor air, increasing the mixture temperature and thus retarding the frosting in the low-pressure evaporators by changing air inlet conditions without additional cost. In addition, the warm exhaust air, driven by the 2 exhaust air fans, is utilized to defrost without compressor operation, which can get rid of the high power consumption of the reverse cycle defrosting method and overcome the limitation of the compressor shutdown defrosting method.

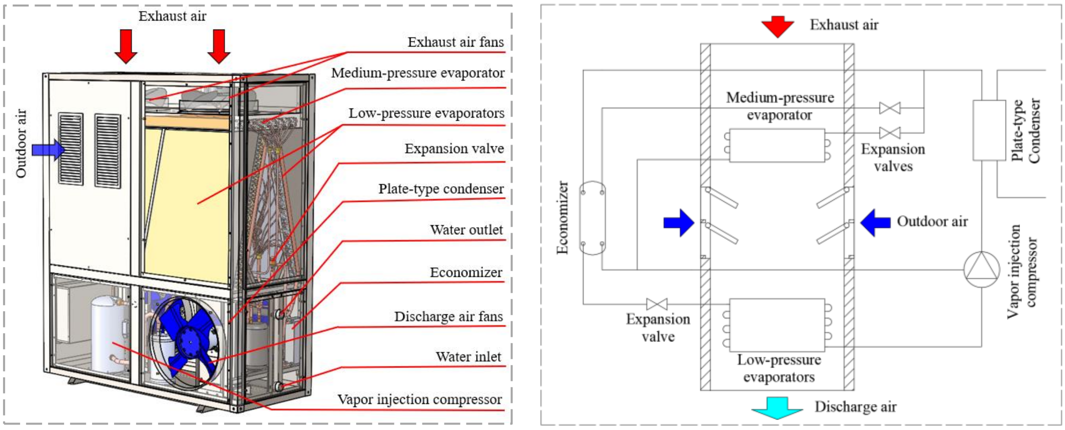

(a) (b)

Figure 1. Structure of the DSHP (a) Inner structure of the DSHP (b) System diagram of the DSHP

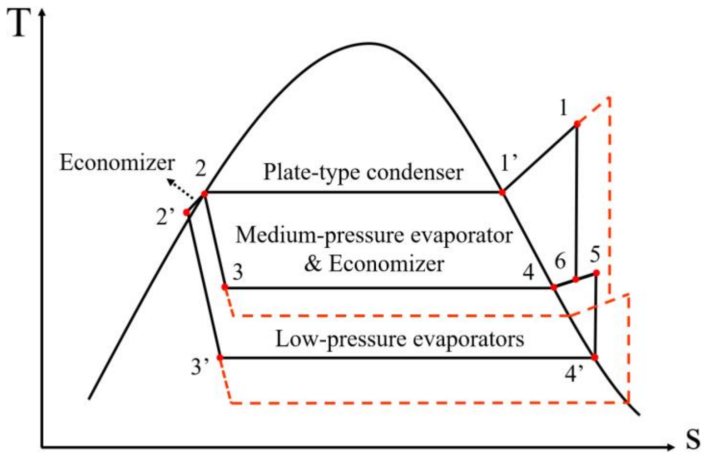

Figure 2. The temperature-entropy diagram of the DSHP

Table 1. Energy flow and balance of the DSHP

Components	Energy and mass conservations
Plate-type condenser	$\dot{m}_{\mathrm{tot}}\left(\frac{(T_1+T_{1'})(s_1-s_{1'})}{2}+T_2(s_{1'}-s_2)\right)=Q_{\mathrm{con}}$
Low-pressure evaporator	$\dot{m}_1 T_{3'}(s_{4'}-s_{3'})=Q_{\mathrm{LE}}$
Medium-pressure evaporator	$\dot{m}_{2'} T_3(s_4-s_3)=Q_{\mathrm{ME}}$
Economizer	$\dot{m}_{2''} T_3(s_4-s_3)=\dot{m}_1\frac{(T_2+T_{2'})(s_2-s_{2'})}{2}$
Vapor injection compressor	$Q_{\mathrm{con}}-Q_{\mathrm{ME}}-Q_{\mathrm{LE}}=W$
	$\dot{m}_1+\dot{m}_2=\dot{m}_{\mathrm{tot}}$
	$\dot{m}_{2'}+\dot{m}_{2''}=\dot{m}_2$

As Figure 3 shown, the manufactured DSHP prototype was optimized and tested in the environmental laboratory where different environmental conditions and water conditions can be simulated by the air conditioning unit and thermostatic water system. Regarding the experiment process, the optimum charge of refrigerant (R410a) of 13 kg was first obtained by considering COP under a fixed condition of outdoor temperature/water outlet temperature of -12 ^{o}C/55 ^{o}C. Subsequently, the optimum COPs of the DSHP prototype were optimized under various working conditions (as listed in Table 2) by adjusting the expansion valve opening. Finally, the optimum expansion valve openings were programmed into the control panel, ensuring the best COP of the DSHP all the time.

To evaluate the heating performance of the DSHP, the heating power consumption (w_{h}) of the DSHP is measured by a high-accuracy power meter, and the heating capacity of the DSHP is calculated by:

$$Q=C_{\mathrm{p}}m\left(T_{\mathrm{water,outlet}}-T_{\mathrm{water,inlet}}\right) \tag{1}$$

where Q is heating capacity, C_p is the isobaric specific heat capacity of water, m is the water mass flow rate, and $T_\mathrm{water,outlet}$ and $T_\mathrm{water,inlet}$ are the water outlet and inlet temperature of the DSHP, respectively.

The COP of the DSHP therefore can be calculated by:

$$COP = \frac{Q}{w_\mathrm{h}} \tag{2}$$

The uncertainty in the measured data is related to the accuracy of the sensor, and the uncertainty in the calculated data accumulates due to the transferability of the uncertainty in the measured data [24], which is expressed as:

$$U_\mathrm{Q} = \left[\left(\frac{\partial Q}{\partial m}U_m\right)^2 + \left(\frac{\partial Q}{\partial T_\mathrm{water,outlet}}U_{T_\mathrm{water,outlet}}\right)^2 + \left(\frac{\partial Q}{\partial T_\mathrm{water,inlet}}U_{T_\mathrm{water,inlet}}\right)^2\right]^{0.5} \tag{3}$$

$$U_\mathrm{COP} = \left[\left(\frac{\partial COP}{\partial Q}U_\mathrm{Q}\right)^2 + \left(\frac{\partial COP}{\partial w_\mathrm{h}}U_{w_\mathrm{h}}\right)^2\right]^{0.5} \tag{4}$$

Eventually, the uncertainty of the measured data and calculated data are listed in Table 3.

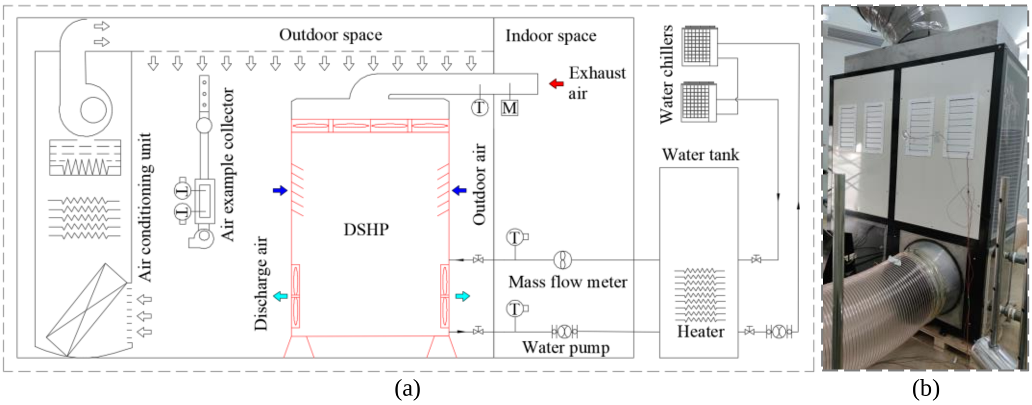

Figure 3. Experimental setup (a) Environmental laboratory (b) the DSHP prototype in experiments

Table 2. Experiment conditions of the DSHP prototype

Refrigerant charge (kg)	Water flow rate (m^3/h)	Exhaust air flow rate (m^3/s)	Exhaust air temperature (°C)	Outdoor air temperature (°C)	Water outlet temperature (°C)
13	4	0.75-1.30	20-25		41
				-12	48
					55
					41
				-6	48
					55
					41
				0	48
					55
					41
				6	48
					55
					41
				12	48
					55
					41
				18	48
					55

Table 3. Uncertainty of experimental data

Sensors	Parameters	Uncertainty
PT-1000	Water outlet temperature of the DSHP ($T_{\text{water,outlet}}$, ºC)	± 0.15 ºC
PT-1000	Water inlet temperature of the DSHP ($T_{\text{water,inlet}}$, ºC)	± 0.15 ºC
Mass flow meter	Water mass flow rate (m, m^3/h)	± 0.5 %
Power meter	Power consumption of the DSHP (W, kW)	± 0.2 %
-	Heating capacity of the DSHP (Q, kW)	± 4.27 %
-	Coefficient of performance of the DSHP	± 4.28 %

2.2 Description of the novel DSHP heating system and comparison systems

As mentioned above, the traditional GB heating system used in most old buildings wastes exhaust air during operation, while the conventional HP heating system, which integrates heat pumps with MVHRs, increases the system complexity and the heating bill of building heating. To solve the application challenges of the conventional HP heating system, the proposed novel DSHP heating system has its own built-in ventilation heat recovery fans. When deploying the novel DSHP heating system to an office, as Figure 4 shown, the required fresh air flows into the office from the right inlet, while the exhaust air is extracted by the DSHP through the left air duct. The DSHP recovers the waste heat from the exhaust air along with absorbing the heat from outdoor air, achieving increasing heating capacity and COP, and then the produced hot water will be used to heat the indoor space through the radiators. The novel DSHP system conducts space heating with improved performance and fulfils the ventilation requirements of the office without additional MVHR at the same time, which efficiently reduces the complexity of the whole heating system. For simplicity, the novel DSHP heating system is called system-A.

Figure 5 shows the structure of the aforementioned conventional HP heating system, which integrates a conventional HP with an MVHR to achieve carbon reduction in the current market. The conventional HP extracts heat from a single heat source, i.e., the outdoor air, and then transfers the heat into the water for space heating through radiators. The ventilation requirement is satisfied by the additional MVHR, which extracts the exhaust air and recovers the waste heat by transferring it to the fresh air. It is clear that the conventional HP heating system has higher complexity than system-A. In this study, the conventional HP heating system is named system-B.

Figure 6 illustrates the traditional GB heating system, which is the most common heating system in current buildings. The GB heats the water and supplies heat to the office through the radiators. Due to the low price of natural gas, the traditional GB heating system does not consume additional electricity for heat recovery, and the ventilation requirement is committed by the exhaust air fans and fresh air inlet which is similar to that of system-A. For simplicity, the traditional GB heating system is called system-C, which is the baseline of the following comparisons.

In the simulation, the three different heating systems will be separately applied to the same office of which structure details are listed in Table 4. The ventilation strategy of the office is according to the ASHRAE recommended air ventilation rate of offices, which is 2 air changes/h [25], so the exhaust air flow rate is 0.8 m^3/s for the office, which is achievable for the proposed DSHP prototype. Furthermore, the internal heat generation comes from the simulated activity schedule which includes 20 workers and 20 computers with fixed working hours (9:00-19:00).

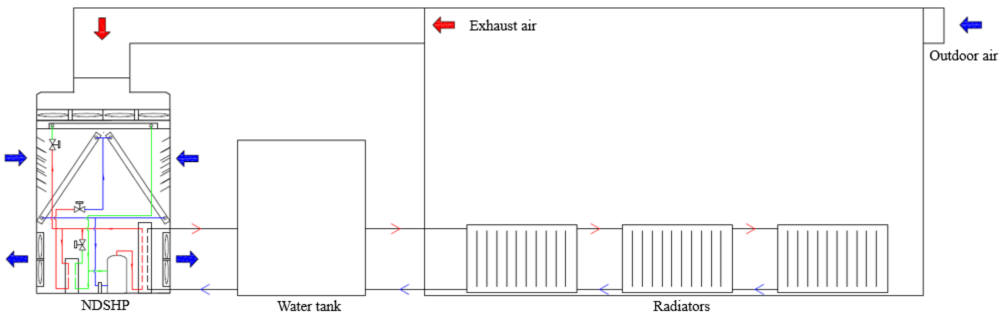

Figure 4. Structure diagram of system-A

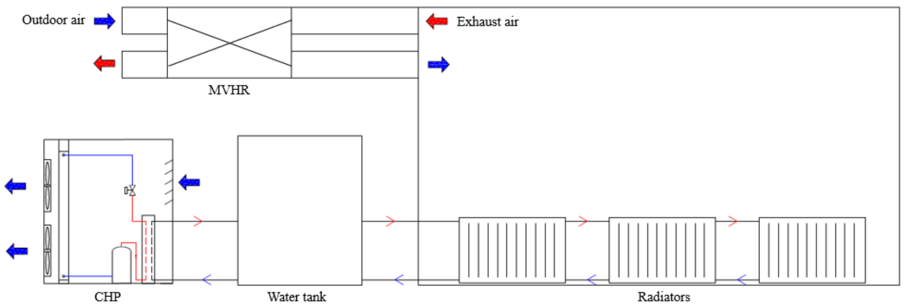

Figure 5. Structure diagram of system-B

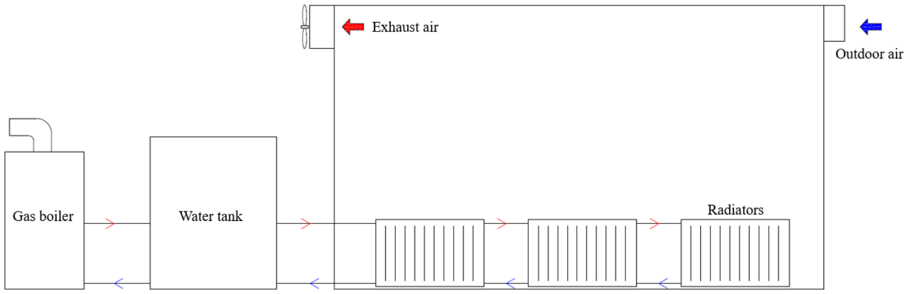

Figure 6. Structure diagram of system-C

Table 4. Parameters details of the office

Area (W*L*H)	Ventilation requirement	Internal heat sources	Building constructions		
			Envelopes	Heat transfer coefficient	Remarks
30 m * 13.3 m * 3.6 m	2 Ach (0.8 m^3/s)	20 workers and 20 computers	Wall	0.1833 $W/m^2/K$	The normal of the main facade is at an angle of 45° to the south.
			Roof	0.5500 $W/m^2/K$	There are no windows on the roof.
			Floor	0.7322 $W/m^2/K$	The floor is in contact with the ground.
			Windows	3.4573 $W/m^2/K$	The window-wall ratios of the main and back façades are 0.2, and that of the left and right façades are 0.

3. Mathematical model of building heating systems

Figure 7 illustrates the modelling flow chart of the heat pump heating systems, i.e., system-A and system-B. The proposed simulation model is based on the following assumptions: (1) The internal heat gains of the office are fixed during working hours; (2) The heat losses from the heating system to the ambience are ignored; (3) The heat supply terminals are enough to deliver the heating amount of system to the office; and (4) The HP water outlet temperature of the heating system are assumed at constant average values. The simulation begins with data loading and input with time steps of one hour. The loaded practical weather data includes hourly outdoor temperatures, hourly global horizontal irradiation (GHI) and hourly diffuse horizontal irradiation (DHI), which are collected from the EnergyPlus database. Thereafter, the building details are inputted followed by ventilation and activity schedule setup. According to the details of the building and the weather data, the hourly heat transfer rate (*HT*) of building envelopes and ventilation, as well as the solar heat gains (H_{sol}) and internal heat gains (H_{int}) are obtained.

After the data loading and input, the whole heating system is simulated by the 5R1C model based on ISO13790 [26]. As Figure 8 depicted, the 5R1C model concludes the whole heating system in an equivalent three-node resistance-capacitance network, which consists of building thermal mass node (T_{th}), indoor surface node (T_{suf}), indoor air node (T_{in}), and capacitance of building thermal mass (C_{th}). The heat transfer between two nodes is related to the temperature of each node and the heat transfer rate (*HT*) between nodes. In each hour, the whole heating system model achieves an energy balance where the heat load and heat gain of each node are equal and expressed as:

$$H_{\text{heat}} + H_{\text{in}} + HT_{\text{fi}}(T_{\text{fresh}} - T_{\text{in}}) = 0 \tag{5}$$

$$H_{\text{suf}} + HT_{\text{os}}(T_{\text{out}} - T_{\text{suf}}) + HT_{\text{si}}(T_{\text{in}} - T_{\text{suf}}) + HT_{\text{ts}}(T_{\text{th}} - T_{\text{suf}}) = 0 \tag{6}$$

$$H_{\text{th}} + HT_{\text{ot}}(T_{\text{out}} - T_{\text{th}}) + HT_{\text{ts}}(T_{\text{suf}} - T_{\text{th}}) + C_{\text{th}} = 0 \tag{7}$$

After the confirmation of the heating setpoint temperature (T_{set}), the hypothetical indoor temperature $T_{\text{h,i}}$ is calculated by assuming the office has no heat supply from the heating system, i.e., $H_{\text{heat}} = 0$, and then the operation mode of the heating system can be judged by comparing the indoor temperature setpoint T_{set} with the hypothetical indoor temperature $T_{\text{h,i}}$. If $T_{\text{h,i}}$ is not lower than T_{set}, the office does not need a heat supply from the heating system, and it is no heating energy consumption during the *i* th hour. Therefore, the indoor temperature $T_{\text{in,i}}$ is finally equal to $T_{\text{h,i}}$. Otherwise, the office needs a heat supply, and thus, based on the 5R1C model, the heating load of the office (L_{i}) will be calculated by considering that the indoor temperature is equal to T_{set}. In addition, the maximum heating amount of the heating system will be evaluated by considering the influence of frosting which appears at conditions of outdoor temperature lower than 5 ºC, and can be expressed as:

$$H_{\text{m,i}} = Q_{\text{i}} t_{\text{m,h,i}} \tag{8}$$

$$t_{\text{m,h,i}} = 1 - r \tag{9}$$

where Q_{i} is the heating capacity of the heat pump, $t_{m,h,i}$ is the maximum heating time. and r is the defrosting time ratio of the heat pump, which is equal to 0 when there is no frosting.

By comparing the heating load of the office and the maximum heating amount of the heating system, the indoor temperature can be identified at last. If $H_{\text{m,i}}$ is larger than or equal to L_{i}, the heating system can fully handle the heating load. So, the heating amount H_{i} of heating system will be adjusted to L_{i} by shorting the operation time during the *i* th hour, so $T_{\text{in,i}}$ can be finally maintained at T_{set}. If $H_{\text{m,i}}$ is less than L_{i}, the heat pump cannot satisfy the heating load of the office. In this condition, H_{i} will be equal to $H_{\text{m,i}}$, and $T_{\text{in,i}}$ will be recalculated according to the 5R1C model.

Once the H_{i} is confirmed, the system's energy consumption W_{i} in the *i* th hour can be calculated by:

$$W_{\text{i}} = W_{\text{h,i}} + w_{\text{d}} t_{\text{d,i}} + W_{MVHR} \tag{10}$$

$$W_{\text{h,i}} = \frac{H_{\text{i}}}{COP_{\text{i}}} \tag{11}$$

$$t_{\text{h,i}} = \frac{H_{\text{i}}}{H_{\text{m,i}}}(1 - r) \tag{12}$$

$$t_{\text{d,i}} = \frac{H_{\text{i}}}{H_{\text{m,i}}} r \tag{13}$$

where COP_{i} is the coefficient of performance of the heat pump unit, $W_{\text{h,i}}$ is the heating energy consumption in kWh, w_{d} is the defrosting power consumption in kW, $t_{\text{h,i}}$ is the actual heating time of the heat pump, $t_{\text{d,i}}$ is the actual defrosting time of the heat pump, and W_{MVHR} is the energy consumption of MVHR.

In this study, an MVHR is applied to system-B to fulfil the fresh air requirement, whose average power consumption is presumed to be at 2.98 kW with an average heat recovery rate of 84.5% during application according to a commercial product manual [27]. Additionally, the heating capacity Q_{i} and COP_{i} of heat pumps are simulated by multiple linear regression equations based on the experiment data of the DSHP prototype and a commercial HP. In the simulation, the average water outlet temperature of the heat pumps is assumed to be 55 ºC, while the outdoor temperature varies with the practical weather data. In each iteration of *i* th hour, the thermal mass temperature $T_{\text{th,i}}$ will be sorted out, which will be the important parameter for $L_{\text{i+1}}$ calculation. By iterating the hourly heating performance of the systems over a full year (8760 hours), the monthly average performances of the three systems are analysed as follows:

Firstly, different from the experiment in the lab, the applied heat pump will experience heating processes and defrosting processes in its long-term operation. Therefore, a seasonal coefficient of performance (SCOP) is used to evaluate the long-term performance of heat pumps in the simulation, which can be expressed as:

$$SCOP_{\mathrm{j}} = \frac{\sum_{i=n}^{m} H_{\mathrm{i}}}{\sum_{i=n}^{m} (W_{\mathrm{h,i}} + w_{\mathrm{d}} t_{\mathrm{d,i}})} \tag{14}$$

where H_{i} is the heating amount, $W_{\mathrm{h,i}}$ is the heating energy consumption, $w_{\mathrm{D,d}}$ is the defrosting power consumption, and $t_{\mathrm{d,i}}$ is the defrosting time of the heat pump during the *i* th hour.

At the system level, the seasonal performance factor (*SPF*) is used to estimate the long-term operating performance of the whole heating system, which is calculated as:

$$SPF_{\mathrm{A,j}} = \frac{\sum_{i=n}^{m} H_{\mathrm{i}}}{\sum_{i=n}^{m} \left(W_{\mathrm{h,i}} + w_{\mathrm{d}} t_{\mathrm{d,i}}\right)} \tag{15}$$

$$SPF_{\mathrm{B,j}} = \frac{\sum_{i=n}^{m} H_{\mathrm{i}}}{\sum_{i=n}^{m} \left(W_{\mathrm{h,i}} + w_{\mathrm{d}} t_{\mathrm{d,i}} + W_{\mathrm{MVHR,i}}\right)} \tag{16}$$

In addition, the monthly heating amount, monthly heating bill and monthly carbon emissions of the system are respectively evaluated as:

$$H_{\mathrm{j}} = \sum_{\mathrm{i=n}}^{\mathrm{m}} H_{\mathrm{i}} \tag{17}$$

$$B_{\mathrm{j}} = \alpha_{\mathrm{e}} \sum_{\mathrm{i=n}}^{\mathrm{m}} W_{\mathrm{i}} \tag{18}$$

$$C_{\mathrm{j}} = \varepsilon_{\mathrm{e}} \sum_{\mathrm{i=n}}^{\mathrm{m}} W_{\mathrm{i}} \tag{19}$$

where H_{j}, B_{j}, C_{j} are the monthly heating amount, monthly heating bill, and monthly carbon emission of system-A and system-B during the *j* th month, respectively, α_{e} and ε_{e} are electricity price and carbon emission factor of electricity, respectively.

Regarding system-C, its heating load is equal to system-A in the simulation, because they are applied to the same office and have the same ventilation method which drives outdoor fresh air directly into the office without preheating. Thus, the gas boiler of system-C has the same heat supply amount as the DSHP, i.e., $H_{\mathrm{C,j}} = H_{\mathrm{A,j}}$. The heating efficiency of the gas boiler (η_{GB}) is presumed as 85% [28, 29], and the seasonal performance factor of system-C ($SPF_{\mathrm{C,j}}$) is equal to be 0.85 by neglecting of the small power consumption of the exhaust air fan. Thereafter, the monthly heating amount, monthly heating bills, and monthly carbon emissions of system-C can be calculated by:

$$SPF_{\mathrm{C,j}} = 0.85 \tag{20}$$

$$B_{\mathrm{c,j}} = \alpha_{\mathrm{g}} \frac{H_{\mathrm{c,j}}}{SPF_{\mathrm{C,j}}} \tag{21}$$

$$C_{\mathrm{j}} = \varepsilon_{\mathrm{g}} \frac{H_{\mathrm{c,j}}}{SPF_{\mathrm{C,j}}} \tag{22}$$

where α_{g} and ε_{g} are natural gas price and carbon emission factor of gas, respectively.

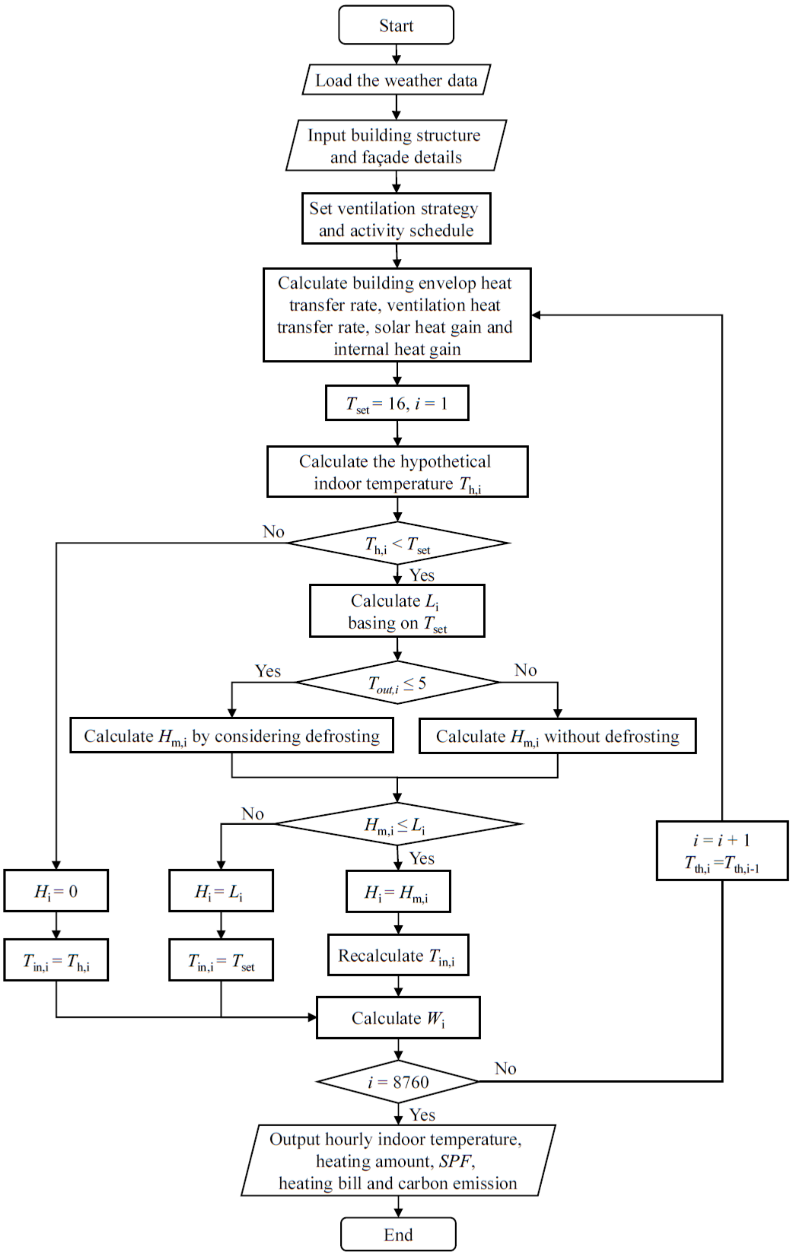

Figure 7. Modelling flow chart of the heat pump heating systems

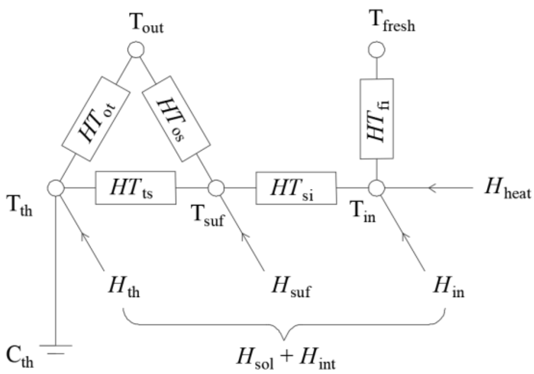

Figure 8. The 5R1C building heating model

4. Results and discussions

4.1 Experiment results and mathematical models of the DSHP and conventional HP

The manufactured DSHP prototype was optimized in the environmental laboratory, whose optimized results are shown in Figure 9 (a), indicating that the highest heating capacity of the DSHP prototype is 39.12 kW at 18 °C/55 °C (outdoor temperature/water outlet temperature), while the highest COP is 4.12 at 18 °C/41 °C. The heating capacity of the DSHP decreases smoothly as outdoor temperature decreases. For instance, at 55 °C water outlet temperature conditions, the heating capacity reduces by 30.42% when the outdoor temperature is cooled down from 18 °C to -12 °C. The power consumption of the DSHP has little change with outdoor temperature but increases a lot with water outlet temperature. Therefore, the COP of the DSHP decreases as outdoor temperature declines, but, for instance, only has a 31.33% deterioration when outdoor temperature changes from 18 °C to -12 °C at a water outlet temperature of 55 °C. It is worth noting that compared to the previous prototype which has been proved in laboratory conditions of -5 °C/30 °C [23], the presented DSHP achieves the maximum water outlet temperature of 55 °C at an extremely cold outdoor temperature of -12 °C, of which heating performance already gratified the requirement of replacing the traditional gas boiler heating system in practical building heating.

The experiment results of the applied conventional HP are listed in Figure 9 (b), which is collected from the official database of a commercial heat pump [30]. The maximum heating capacity of the conventional HP is 20.24 kW at 20 °C/35 °C, and the highest COP of the HP is 5.89 at 20 °C/35 °C. However, the heating capacity of the HP dramatically decreases as outdoor temperature colds down, which declines by 58.61% when outdoor temperature decreases from 20 °C to -7 °C at 55 °C water outlet temperature. It is noted that the heating capacity of the HP declines as water temperature rises, which is contrary to the trend of the DSHP and is a very important application challenge that the DSHP overcomes. In addition, the power consumption of the HP fluctuates more greatly than that of the DSHP. Eventually, the COP of the conventional HP deteriorates as outdoor temperature decreases, which declines by 47.49% when the outdoor temperature drops from 20 °C to -7 °C at the water outlet temperature of 55 °C, performing more volatility than that of the DSHP.

Defrosting experiments of the DSHP reveal that the defrosting time is 4 mins after every 20 mins at -6 °C/41 °C and 0 °C /41 °C, i.e., 16.67% of defrosting time ratio, and defrosting power consumption is 0.46 kW. The defrosting performance of the presented DSHP coincides with the previous prototype which also consumed a short defrosting time and had negligible defrosting power consumption [23]. The defrosting performance of the conventional HP is not provided by the official database, and thus is presumed according to Song et al. [6] and Vocale et al. [31] investigation that the defrosting time ratio is 20% and the defrosting power consumption is 2/3 of the heating power consumption in the simulation.

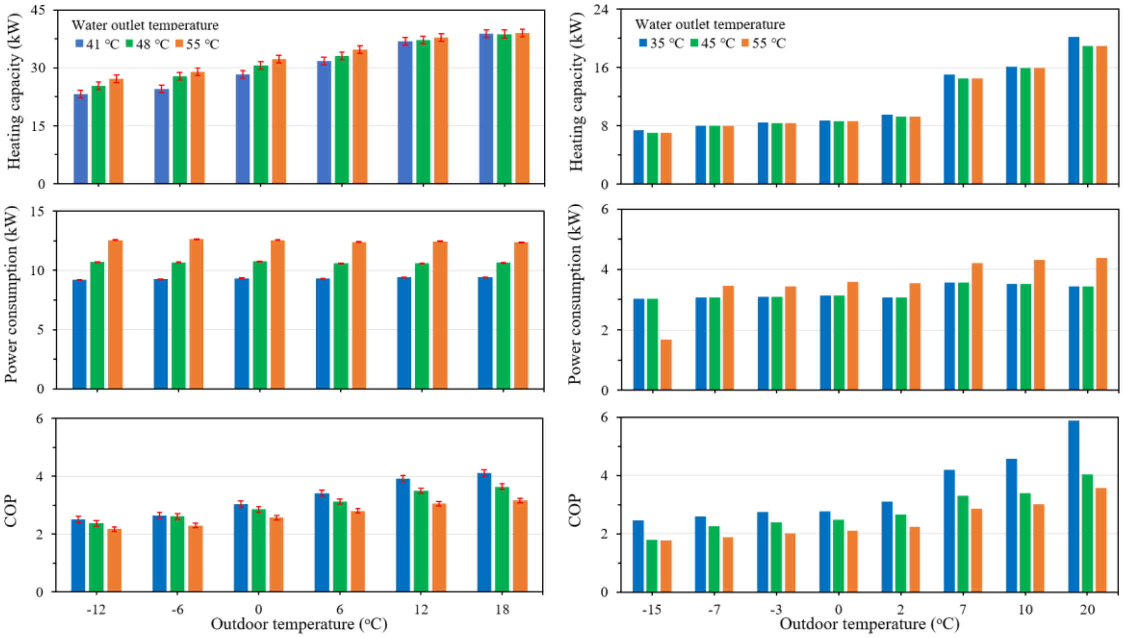

(a) (b)

Figure 9. Experiment results of the different heat pumps (a) the DSHP (b) the conventional HP

As Figure 10 shown, to simulate the performance of the DSHP prototype, Multiple Linear Regression (MLR) is applied to gain the equations of $Q_{\mathrm{D,i}}$ and $COP_{\mathrm{D,h,i}}$ basing on the experiment data. The regression result is illustrated as the grid surface in Figure 10, which highly coincides with the experiment points, and thus can accurately predict the heating performance of the DSHP at various application conditions. As a result, the mathematical model of the

DSHP is expressed as the equations of $Q_{\mathrm{D,i}}$ and $COP_{\mathrm{D,h,i}}$ as followed, whose R^2 (the coefficient of determination) are 0.987 and 0.989, respectively:

$$Q_{\mathrm{D,i}} = 11.3276167069219 + 0.000816133452435193 * T_{\mathrm{out,i}}{}^2 - 0.00358510819903730 * T_{\mathrm{water,i}}{}^2 - 0.0106228325501578 * T_{\mathrm{out,i}} * T_{\mathrm{water,i}} + 0.995435448865903 * T_{\mathrm{out,i}} + 0.573101795701124 * T_{\mathrm{water,i}} \quad (20)$$

$$COP_{\mathrm{D,h,i}} = 3.1425 + 0.000116425040114020 * T_{\mathrm{out,i}}{}^2 - 0.000646128467782338 * T_{\mathrm{water,i}}{}^2 - 0.00171910627919067 * T_{\mathrm{out,i}} * T_{\mathrm{water,i}} + 0.128337485057284 * T_{\mathrm{out,i}} + 0.0251067875765841 * T_{\mathrm{water,i}} \quad (21)$$

Where $T_{\mathrm{out,i}}$ is the outdoor temperature and $T_{\mathrm{water,i}}$ is the water outlet temperature of the *i* th hour.

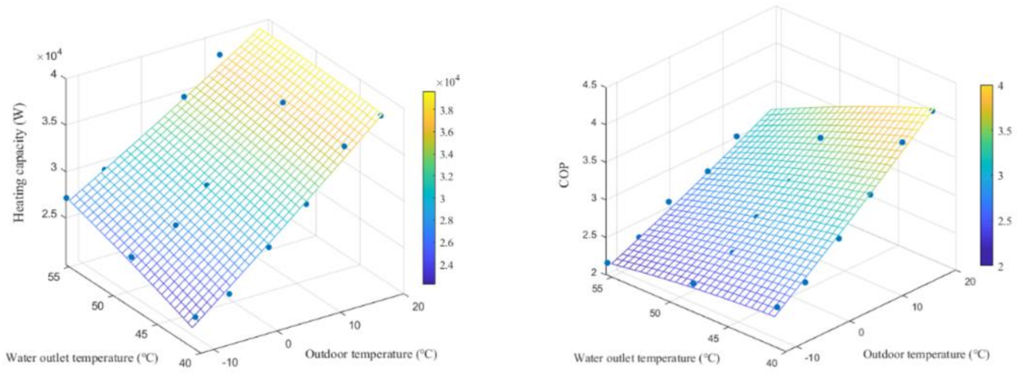

(a) (b)

Figure 10. Performance of the DSHP (a) Heating capacity of the DSHP (b) COP of the DSHP

Regarding the mathematical model of the conventional HP, as Figure 11 shown, based on the MLR of the conventional HP experiment data, the regression surface of $Q_{\mathrm{HP,i}}$ and $COP_{\mathrm{HP,h,i}}$ are consistent with the official data, which are expressed as the following equations. The R^2 (the coefficient of determination) of $Q_{\mathrm{HP,i}}$ and $COP_{\mathrm{HP,h,i}}$ are 0.935 and 0.956, respectively:

$$Q_{\mathrm{HP,i}} = -0.230494643219705 + 0.00460654165351375 * T_{\mathrm{out,i}}{}^2 - 0.00789221429429487 * T_{\mathrm{water,i}}{}^2 - 0.00169822548262473 * T_{\mathrm{out,i}} * T_{\mathrm{water,i}} + 0.455228552732591 * T_{\mathrm{out,i}} + 0.583133882110729 * T_{\mathrm{water,i}} \quad (22)$$

$$COP_{\mathrm{HP,h,i}} = 8.63921319787365 + 0.00138611842808078 * T_{\mathrm{out,i}}{}^2 + 0.00189956186875287 * T_{\mathrm{water,i}}{}^2 - 0.00257243315879058 * T_{\mathrm{out,i}} * T_{\mathrm{water,i}} + 0.185811944733147 * T_{\mathrm{out,i}} - 0.221346571606090 * T_{\mathrm{water,i}} \quad (23)$$

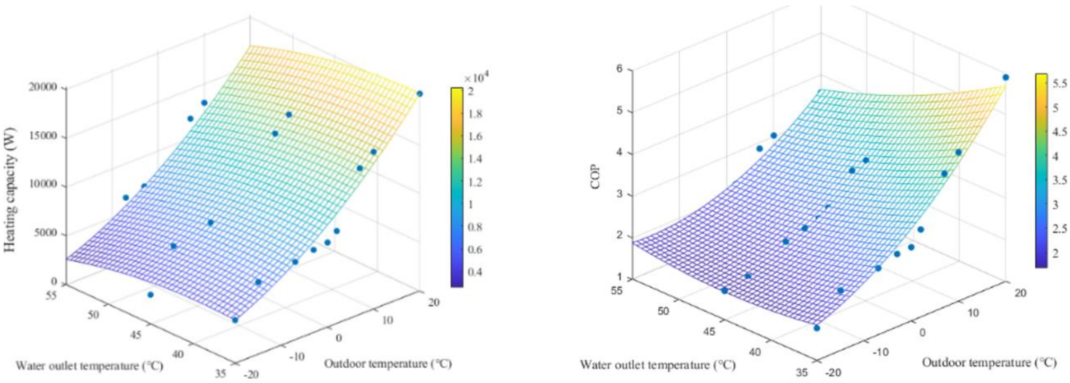

(a) (b)

Figure 11. Performance of the HP (a) Heating capacity of the HP (b) COP of the HP

4.2 Simulation results and comparisons of different building heating systems

4.2.1 Annual performances comparisons of the three different building heating systems

In this section, the three heating systems are simulated and compared on a monthly and annual basis in London's weather conditions. Notably, aiming to investigate the application characteristics of different heat pump heating systems, including the heating performance and defrosting performance, the deployment amounts of the heat pump of different systems are matched to the condition of average office temperature above 16 ºC [32]. Eventually, the matching result of the DSHP is 1 in system-A and that of the conventional HP is 3 in system-B. As a result, Figure 12 illustrates the monthly average outdoor temperatures and indoor temperatures of the three systems, where the outdoor temperature of London achieves the lowest point of 3.94 ºC in February and peaks at the highest point of 17.31 ºC in July. The indoor temperature of all heating systems can maintain at 16 ºC during the main heating month, i.e., October to April, and rises above 16 ºC in other months because of no cooling supply. It reveals that the three systems have a good heating capacity to satisfy the heating load of the office and maintain indoor thermal comfort.

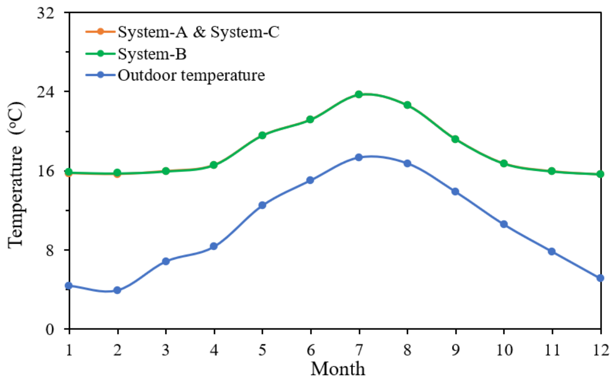

Figure 12. The monthly indoor temperature of different systems

Figure 13 illustrates the heating amount of the three different heating systems. The main heating months of the three systems are all between October and April when the outdoor temperature and solar radiation are low in London. The heating amount of system-A ($H_{\mathrm{A,j}}$) and system-C ($H_{\mathrm{C,j}}$) peaks at 6434.76 kWh in January, and reaches the minimum of 21.64 kWh in July when there are only a few cold days that need some heat supply. The maximum and minimum heating amount of system-B ($H_{\mathrm{B,j}}$) appear in the same months, which are 3222.09 kWh and 7.84 kWh, respectively. Notably, $H_{\mathrm{B,j}}$ is always smaller than $H_{\mathrm{A,j}}$ and $H_{\mathrm{C,j}}$ due to the MVHR recovering waste heat from exhaust air to fresh air, resulting in a 30.07% to 51.71% decrease in $H_{\mathrm{B,j}}$ when compared to $H_{\mathrm{A,j}}$ and $H_{\mathrm{C,j}}$. However, although the MVHR reduces the heating amount of system-B, the final eco-economic performances of the systems need to be combined with the *SPF* of the systems to consider comprehensively.

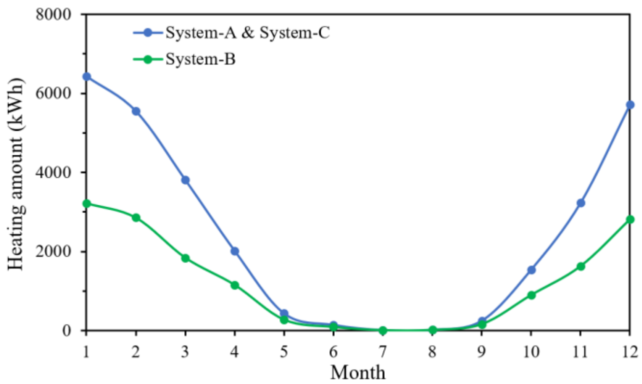

Figure 13. Monthly heating amount of different systems

Figure 14 represents the simulation results of the SPF_{j}. It is noted that the SPF_{A} is equal to $SCOP_{\mathrm{DSHP}}$ according to the equations (11) and (12), owing to the simplicity of system-A that does not has additional energy consumption from other equipment. From the simulation results, $SPF_{\mathrm{A,j}}$ is significantly better than $SPF_{\mathrm{B,j}}$ and $SPF_{\mathrm{C,j}}$ throughout the year, which peaks at 3.03 in August when the monthly average outdoor temperature reaches its highest point. In the coldest month, i.e., February, $SPF_{\mathrm{A,2}}$ is 2.69, which still maintains 89.00% of the highest point. Regarding system-B, the system energy consumption consists of the conventional HP and MVHR. So, $SPF_{\mathrm{B,j}}$ and $SCOP_{\mathrm{HP,j}}$ are not equal according to the equations (11) and (13). It is found that the $SCOP_{\mathrm{HP}}$ ranges from 2.15 to 3.03, which only maintains 70.89% of the highest point in the coldest month. Therefore, the conventional HP performs badly as the weather gets colder, while the DSHP can operate stably for the whole year. As a result, the DSHP had a maximum improvement of 25.62% in the *SCOP* in January when compared to the conventional HP. When it comes to the performance of system-B, i.e., $SPF_{\mathrm{B,j}}$, the poor $SCOP$ of the conventional HP and the additional energy consumption of the MVHR eventually result in the poor $SPF_{\mathrm{B,j}}$, which reaches the highest point of 1.28 in January and hits the lowest point of 0.45 in July. As for system-C, $SPF_{\mathrm{C,j}}$ is constant at 0.85 which is the comparison baseline.

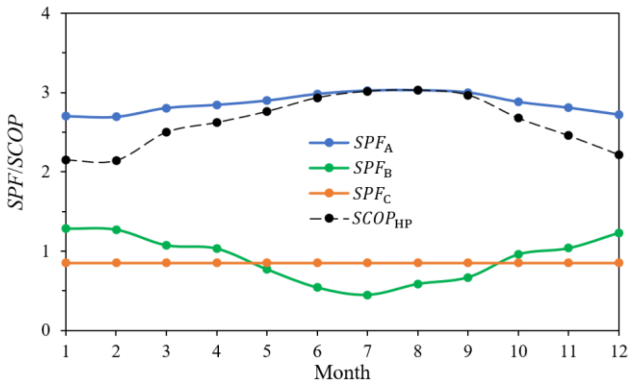

Figure 14. The monthly average efficiency of different systems

By comprehensively considering the influence of heating amount and *SPF*, the eco-economic performances of different systems are analysed and compared as follows. To estimate the environmental and economic performance of different systems, the annual average electricity price and natural gas price in the UK are obtained from Bionic Services Ltd [33], which are £0.143 per kWh and £0.045 per kWh for medium businesses, respectively. And the carbon emission factors for electricity and natural gas in the UK are 0.176 kg/kWh and 0.183 kg/kWh, respectively, which are provided by the climate transparency report of G20 countries [34] and the greenhouse gas reporting [35].

Figure 15 illustrates that the monthly heating bill of system-A ($B_{\mathrm{A,j}}$) is the lowest over the year. The minimum and maximum of $B_{\mathrm{A,j}}$ are in July and January, which are £0.65 and £340.43, respectively. The monthly heating bills of system-B ($B_{\mathrm{B,j}}$) are between £2.50 and £359.46, which are £1.8 to £60.29 higher than that of system-A. When it comes to system-C, $B_{\mathrm{C,j}}$ varies from £0.72 to £340.66, which is slightly higher than that of system-A, but £1.78 to £53.77 lower than that of system-B. The continuously higher heating bills of system-B obstruct the deployment of low-carbon heating systems and the process of building decarbonization. The proposed novel DSHP heating system successfully reduces the heating bills and the system complexity of the conventional HP heating systems, which overcomes the challenges of heating decarbonization and makes the low-carbon heating system market-competitive.

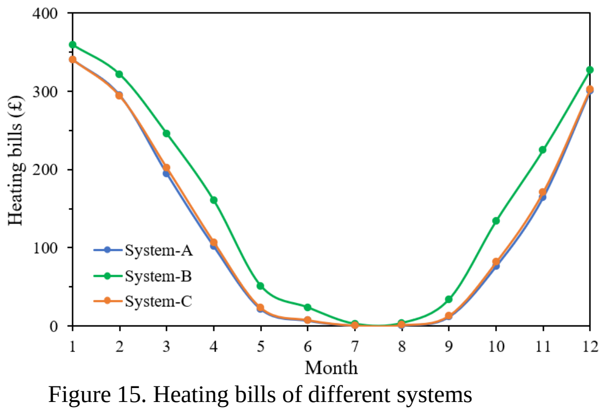

Figure 15. Heating bills of different systems

Figure 16 depicts that system-A produces the least carbon emissions owing to its high system efficiency and low energy consumption, which ranges from 0.79 kg to 419.23 kg in the simulation year in London. System-B produces 3.08 kg to 442.66 kg of carbon emissions, which is 5.59% to 287.71% higher than that of system-A. Regarding system-C, it is shown that the gas boiler produces an enormous amount of carbon emissions ranging from 2.15 kg to 967.65 kg, which is 229.73% to 270.46% higher than that of system-A. It is clear that the gas boiler heating system is the key obstacle to decarbonizing buildings. The DSHP can significantly decline carbon emissions and save the bill of building heating, which is the best substitute for gas boilers.

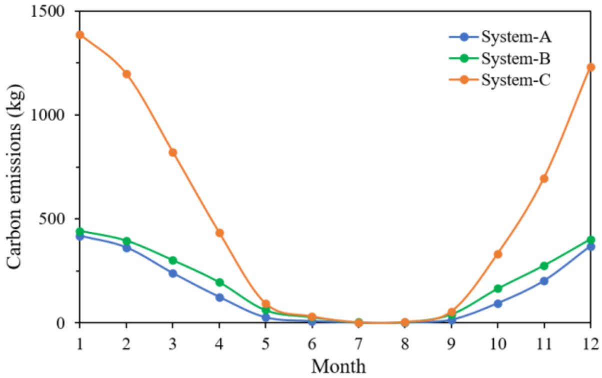

Figure 16. Carbon emissions of different systems

According to the monthly performance of systems, annual performance analyses are further carried out in Figure 17. Benefiting from the novel defrosting method, system-A achieves near-zero defrosting cost, which only accounts for 0.31% of the total heating bill. However, the reversed defrosting method of the conventional HP results in a high defrosting cost, which accounts for 3.29% of the total annual heating bill of system-B. Eventually, the poorer-performing conventional HP, the more costly defrost method and the additional MVHR costs combine to result in higher annual heating bills for System B, and these negative properties also enlarge the annual carbon emissions of system-B. As a result, system-A significantly saves the annual heating bill by 19.73% (£372.46) and creates a 19.73% (458.67 kg) carbon reduction when compared to system-B, and in the 20-year life cycle, the total bill saving can reach £74449.20 with 9173.45 kg carbon reduction. It is seen that system-A has considerable eco-economic advantages by recovering exhaust waste heat with innovative structure designs.

When it comes to system-C, the traditional non-renewable heating system costs more than system-A and emits numerous carbon dioxides. In comparison, system-A can save 1.94% (£30.02) on the annual heating bill and declines 70.34% (4424.14 kg) carbon emissions per annum, which achieves a negative carbon reduction cost of -£6.79/t in its first. Within the life cycle, system-A can save £600.44 and offers 88482.88 kg carbon reduction when compared to system-C, which is a key promotion for carbon neutrality.

However, compared system-B to system-C, due to the poorer eco-economic performance, system-B reduces carbon emission by 63.05% (3965.47 kg) per year but dramatically increases the heating bill by 22.16% (£342.44), reaching 79309.43 kg carbon reduction at the expenses of £6848.76 additional heating bill in the 20-year life cycle, i.e., the carbon reduction cost of system-B is £86.35/t. The annual eco-economic results indicate that system-A significantly improves the performance and creates application advantages of low-carbon heating systems, which overcomes the deployment challenges of substituting traditional gas boiler heating systems.

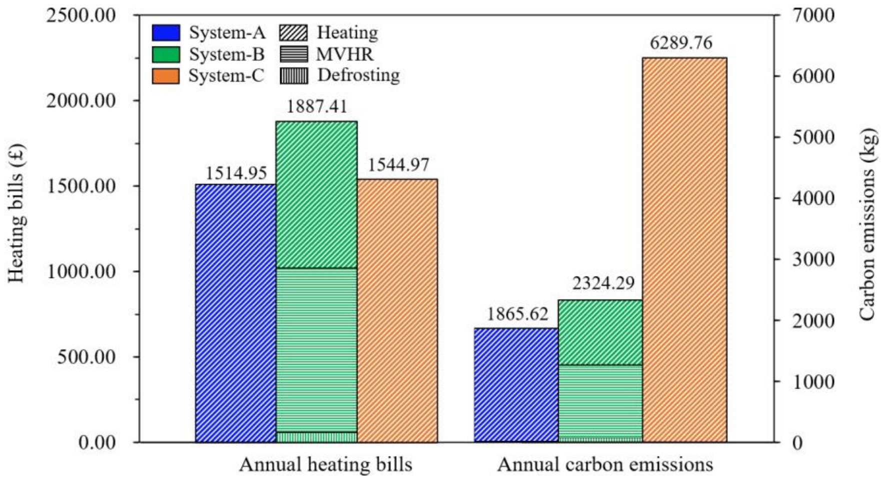

Figure 17. Annual economic and environmental performances of different systems

4.2.2 Application potential analysis of the DSHP heating system in different regions

Decarbonization in building heating is in full swing around the world. However, different regions have distinguished weather conditions and energy strategies, deeply affecting the deployment potential of low-carbon heating systems. Therefore, the economic and environmental performance analysis of the three systems under different regions is important to further discuss the feasibility of the novel DSHP heating system. To suit the working range of the heat pump systems, 8 available regions are selected based on the database of EnergyPlus. Figure 18 illustrates the maximum and minimum monthly average outdoor temperatures of selected regions. The maximum monthly average temperatures of different regions are mainly in July when there is less or no heating load in the office. The minimum monthly average temperature of Japan is down to -3.85 ºC, while that of Spain is 6.16 ºC. Therefore, the selected regions cover a wide range of weather conditions, and the eco-economic performance comparison among the three systems in different regions can depict more insights into the application of the DSHP. Due to the colder climate of the regions when compared to London, the matching amount of the DSHP is 2 and that of the HP is 6 in the select regions to maintain the indoor temperature of the office.

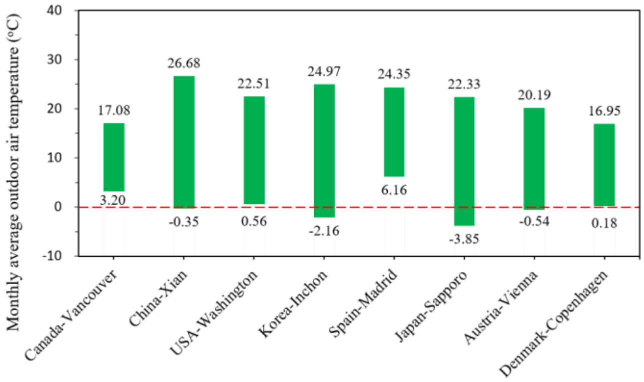

Figure 18. The outdoor temperature of different regions

Figure 19 depicted the simulation results of the annual heating amount of different systems, which are affected by the outdoor temperature, varying in different regions. The heating systems in the coldest Japan supply the largest heating amounts, while those in the warmest Spain have the smallest heating amounts. It is seen that system-B has 45.28% to 49.60% lower heating amounts than system-A and system-C, and the heating amount reduction by MVHR heat recovery is enlarged as the regional weather condition gets colder. However, the lower heating amount does not always translate into bill saving after considering the *SPF* of the systems and energy prices of different regions.

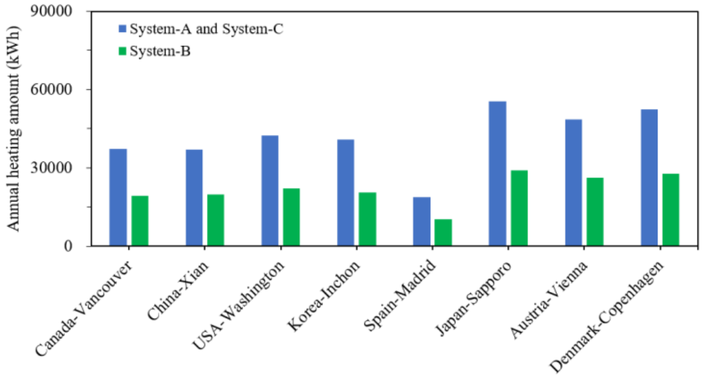

Figure 19. Annual heating amount of the three systems in different regions

From Figure 20 of the *SPF* of different systems, it is seen that system-A keeps the best *SPF* in different regions among the three systems. The *SPF* of different systems are all highly related to the outdoor temperature, so, the maximum SPF_{A} is 2.79 in Spain in which it has the warmest winter, while the SPF_{A} is down to 2.54 in the coldest Japan. The SPF_{B} is ranging from 1.20 to 1.35 in different regions, while that of system-C is constant at 0.85. As a result, The *SPF* of system A increased by 89.42% to 132.87% and 198.46% to 228.09% compared to system B and system C respectively.

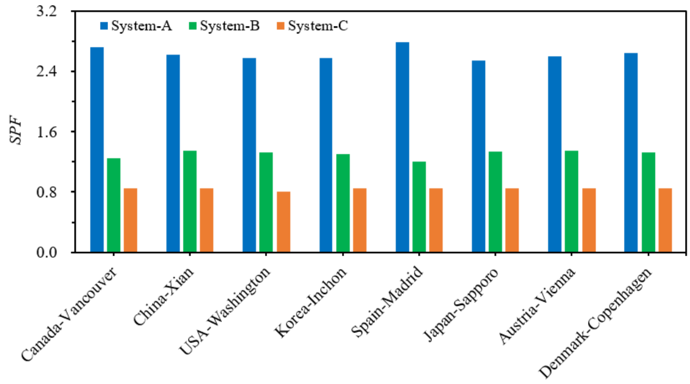

Figure 20. SPF of diff of the three systems in different regions

From Figure 21 of worldwide non-domestic energy prices which are collected from the GlobalPetroprices database, Canada has the lowest natural gas price (£0.020 per kWh) and the second lowest electricity price (£0.082 per kWh after £0.080 per kWh of Korea) among the selected regions, while Denmark has the highest natural gas price (£0.127 per kWh) and electricity price (£0.216 per kWh). And of note is that the electricity prices are obviously higher than natural gas prices in different regions, which has significant effects on heat pumps' economic advantage when compared to gas boilers.

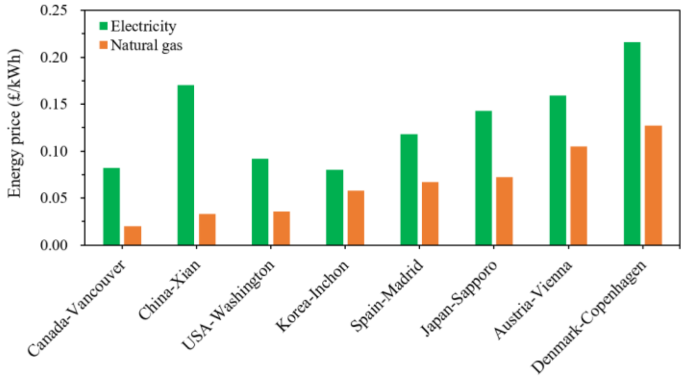

Figure 21. Worldwide energy prices

From Figure 22 of annual heating bills, although the electricity price is always higher than the natural gas price, system-A and system-B are still cost-effective when compared to system-C in most regions. In the USA, Korea, Spain, Japan, Austria and Denmark where the electricity prices are 37.93% to 155.56% higher than gas prices, system-B saves 19.12%, 54.52%, 31.59%, 34.32%, 48.56%, and 42.16% on heating bills respectively when compared to system-C, and the energy-efficient system-A can provide heating bills saving of 20.64%, 54.36%, 46.32%, 33.46%, 50.32%, and 45.35% respectively when compared to system-C. However, in high electricity price regions, i.e., Canada and China, where the electricity prices are respectively 310.00% and 412.05% higher than the natural gas prices, system-B has 45.03% and 72.81% higher heating bills compared to system-C, respectively. Although system-A reduces the heating bill by 11.54% and 3.61% respectively when compared to system-B, it still has 28.29% and 66.56% higher heating bills than system-C in Canada and China, respectively. More importantly, comparisons between system-A and system-B show that system-A has lower heating bills than system-B in most regions which is up to 21.53% in the warmest Spain. But, in the two coldest regions, i.e., Korea and Japan, system-A has 0.36% and 1.31% higher heating bills than system-B, respectively. This is due to the difference between the *SPF* of system-A and system-B being smaller when the regional weather is colder, and finally, system-B achieves bill saving compared to system-A by cooperating with the strong heating load-reducing ability of the MVHR in extremely cold regions.

Table 5 shows the cost distribution of heating bills for different heating systems. Benefiting from the innovative exhaust air defrosting method, the defrosting cost proportion of system-A only ranges from 0.25% to 0.66%, while the minimum defrosting cost proportion of system-B is 2.89% in Spain, and the maximum defrosting cost proportion of system-B is up to 8.99% in Japan. The defrosting cost proportion of system-B is dramatically higher than that of system-A, causing non-negligible deterioration on *SCOP* of the conventional HP and *SPF* of system-B, and thus contributing to the poor economic performance. The costive defrosting method is one of the main problems causing the higher heating bills of system-B, while the impact of novel exhaust air defrosting of the DSHP is near zero in all regions.

To sum up, from the perspective of the economy, the heat pump heating systems deployment potential is severely impacted by the energy prices of different regions because cheap fossil fuel will be a disincentive for consumers to select low-carbon heating systems. Furthermore, the application potential of the novel DSHP heating system needs to be investigated by considering the weather conditions of different regions, which can generate considerable bill saving compared to the conventional HP system in non-extreme cold climate regions.

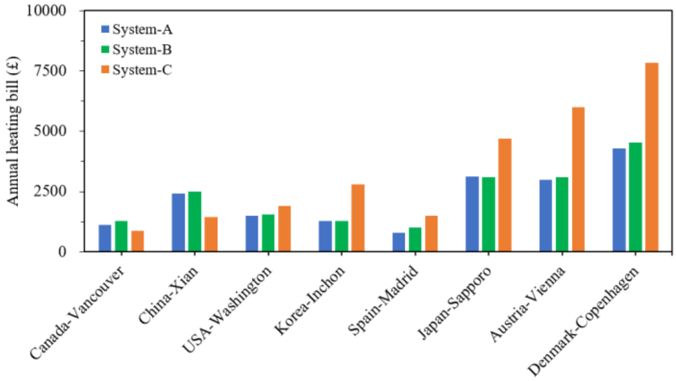

Figure 22. Annual heating bills of the three systems in different regions

Table 5. Cost distribution of heating bills in different regions

Regions	Systems	Heating cost	MVHR cost	Defrosting cost
Canada-Vancouver	System-A	99.59%	0.00%	0.41%
	System-B	51.08%	44.09%	4.83%
	System-C	100.00%	0.00%	0.00%
China-Xian	System-A	99.41%	0.00%	0.59%
	System-B	58.86%	33.15%	7.98%
	System-C	100.00%	0.00%	0.00%
USA-Washington	System-A	99.40%	0.00%	0.60%
	System-B	58.33%	33.79%	7.88%
	System-C	100.00%	0.00%	0.00%
Korea-Inchon	System-A	99.40%	0.00%	0.60%
	System-B	57.86%	34.32%	7.82%
	System-C	100.00%	0.00%	0.00%
Spain-Madrid	System-A	99.75%	0.00%	0.25%
	System-B	47.05%	50.05%	2.89%
	System-C	100.00%	0.00%	0.00%
Japan-Sapporo	System-A	99.34%	0.00%	0.66%
	System-B	60.77%	30.24%	8.99%
	System-C	100.00%	0.00%	0.00%
Austria-Vienna	System-A	99.40%	0.00%	0.60%
	System-B	59.09%	32.81%	8.09%
	System-C	100.00%	0.00%	0.00%
Denmark-Copenhagen	System-A	99.44%	0.00%	0.56%
	System-B	56.57%	36.13%	7.30%
	System-C	100.00%	0.00%	0.00%

Regarding the environmental performance of the three systems, it is highly dependent on the carbon emissions factor (CF) of electricity, which is related to the region's energy policies and is an important parameter indicating the renewability of power generation in different regions. According to the climate transparency report of G20 countries [34] and the greenhouse gas emission report of the European Environment Agency [36], CFs of different regions are illustrated in Figure 23 that the CF of natural gas is 0.183 kg/kWh, while CF of electricity varies from 0.07 kg/kWh to 0.54 kg/kWh. In China, the USA, Korea, and Japan, electricity CFs are 68.59% to 192.07% higher than that of natural gas. In other regions, especially, most Europe countries, their power generation is shifting to less carbon-intensive by using more solar energy and wind energy. Therefore, the electricity CFs of Canada, Spain, Austria, and Denmark are 3.80% to 62.34% lower than that of natural gas.

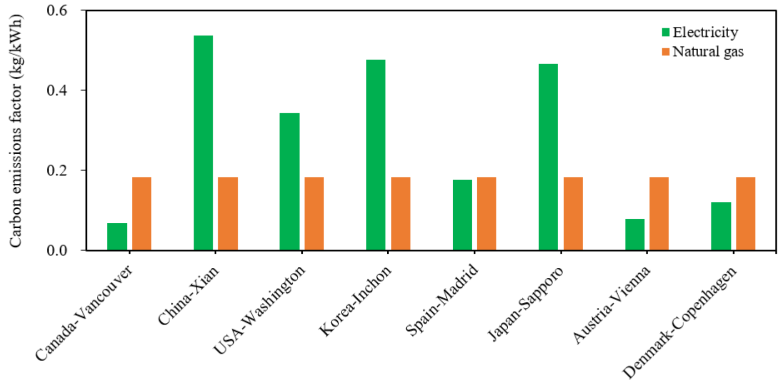

Figure 23. Carbon emissions factor of different regions

From the result of carbon emissions, Figure 24 indicates that the two heat pump heating systems have limited carbon reduction performance when compared to the gas boiler system in the four countries with high electricity CFs, i.e., China, the USA, Korea, and Japan. System-B only reduces annual carbon emissions by 1.43%, 41.04%, 14.71% and 16.28%, respectively, while system-A reduces the carbon emission by 4.99%, 42.15%, 14.39% and 15.18%, respectively, when compared to system-C in China, the USA, Korea, and Japan. When it comes to the countries with low electricity CFs, i.e., Canada, Spain, Austria, and Denmark, the carbon reduction of system-B achieves 62.64% to 86.68% and that of system-A reaches 70.68% to 88.21% when compared to system-C, respectively. Similar to the economic performance results, system-A has better carbon reduction ability than system-B in most regions but performs worse in Korea and Japan.

In summary, the two heat pump heating systems have definitely better environmental performance than gas boiler systems but do not always have preferable economic performance in regions with high electricity prices. The novel DSHP heating system can achieve more heating bill savings and carbon reductions in non-extremely cold regions by recovering exhaust air waste heat and improving *SPF* when compared to conventional HP systems, which is a better substitute for the non-renewable heating device in most regions.

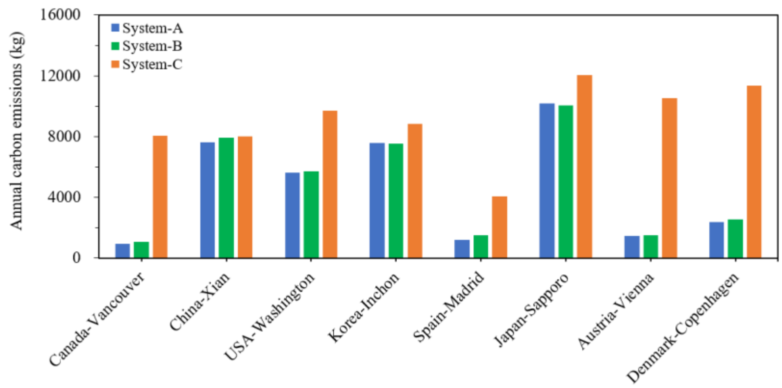

Figure 24. Annual carbon emissions of the three systems in different regions

4.3 *System demonstration and field test results*

A demonstration system applying the DSHP prototype was installed in the Hull central library for practical use, delivering real-life application performance data and simulation validation for the proposed model. The demonstration system shown in Figure 25 depicts that the practical DSHP is deployed on the roof of the library and connected to the serviced office by the black exhaust air duct. The practical DSHP extracts the exhaust air by the duct from the corner window of the office to the top of the DSHP, and then produces hot water and stores it in water tanks by absorbing heat from the exhaust air and outdoor air. The practical office has a similar room structure to the model, and the space heating is conducted by 8 fan coil terminals. The operational data from 4th Jan to 8th Jan 2022 are presented in this paper. The outdoor/indoor temperatures and water outlet temperature were recorded by temperature humidity sensors and platinum resistors in minutes, and the heating amount and energy consumption of the DSHP system were measured and accumulated by using heat meters and current transmitters, respectively. To validate the model, the results of practical weather conditions and working conditions of the demonstration system are listed in Table 6.

Figure 26 shows comparison results of the practical and simulative performance. It is clear that the simulative heating amount of the DSHP heating system was 9.85% higher than the practical result, while the simulative energy consumption was 6.36% lower than the practical result. The simulation deviations are due to unpredictable human activities and internal machine operation in the practical working space during the field test period, which created additional internal heat gain and led to the lower heating amount of the practical DSHP system. Furthermore, in practical application, the DSHP system has additional exposed surfaces from the connection tubes and storage tanks, causing additional heat loss. Therefore, the practical DSHP needed to work longer and consumed more energy to gratify the identical indoor temperature. As a result, the practical *SPF* of the DSHP system is 2.24, which is 14.83% lower than the simulative *SPF*. According to the validation results, the proposed model has good accuracy in predicting the heating performance of the DSHP system.

(a)

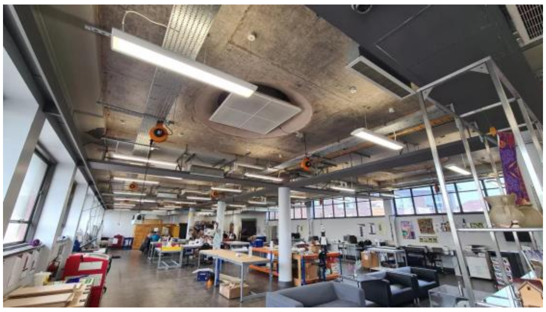

(b)

Figure 25. Practical experiment system (a) DSHP (b) Serviced office

Table 6. Practical experiment conditions

Practical condition	Values
Office geometry (W*L*H, m)	30 * 13.3 * 3.6
Outdoor temperature (°C)	0-7.92
Average working indoor temperature of the office (°C)	19.98
Average working water outlet temperature of DSHP (°C)	56.28

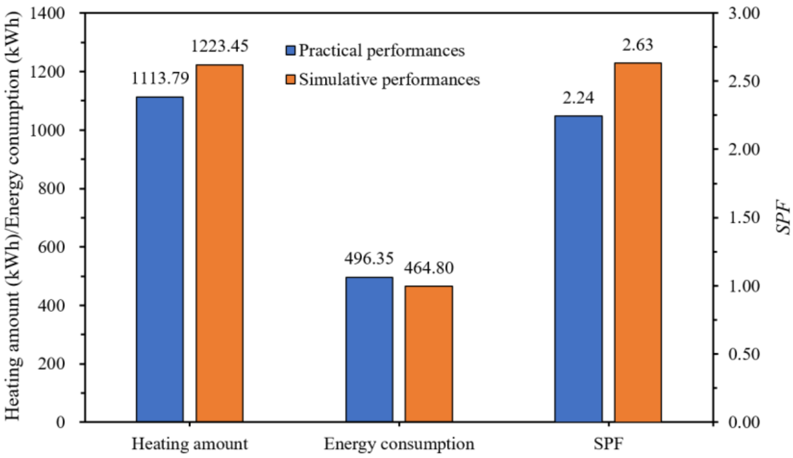

Figure 26. Comparisons between experimental and simulative performances of the DSHP heating system

4.4 *Further remarks*

From the discussions above, the heating performance and eco-economic advantages of the novel DSHP heating system are thoroughly illuminated by comparing them to conventional HP and GB heating systems in different regions. According to the simulation, the innovative construction of the DSHP heating system successfully provides considerable bill savings and carbon reductions in different regions, showing excellent application potential. However, the theoretical results are limited by the model assumptions and practical operation conditions, which are deviations from the actual application. Therefore, the manufactured DSHP need to be further demonstrated in a public building for a long-term application, in which the performance of the novel heating system can be practically testified and revealed for the ambitious carbon neutral targets.

5. Conclusions

An experiment-based model of the DSHP heating system was proposed and validated after the prototype was designed and tested in this study, which performed a good simulative accuracy. Based on the model, three different heating systems. i.e., the novel DSHP heating system (system-A), conventional HP heating system (system-B) and traditional GB heating system (system-C) were simulated and compared in various regions. The annual simulation was conducted to discover the heating performance and characteristics of the DSHP heating system, and then, further comparisons in different regions were presented to reveal the eco-economic performance as well as the application potential of system-A, which is detailed below:

(1) Regarding the system performance and characteristics in London simulation, the DSHP has a stable monthly *SCOP* between 2.69 and 3.03 throughout the year, benefiting from the double heat sources of exhaust air and outdoor air, vapor injection compression, and net-zero consumption defrosting. In the same conditions, the monthly *SCOP* of the conventional HP is fluctuating between 2.15 and 3.03 in the simulation. And thus, the DSHP has higher *SCOPs*, of which the improvement enlarges with the decline of average outdoor temperature and reaches the maximum promotion of 25.62% in the coldest January.

(2) Respecting the eco-economic performance results in London, the system-A provides £0.72 to £7.46 bill saving with 2.15 kg to 967.65 kg carbon reduction when compared to system-C over the year, while the system-B cost £1.78 to £53.77 more than system-C when reducing the carbon emissions by 0.11 kg to 944.22 kg. In the annual results of comparing to system-C, system-A eventually achieves a negative carbon reduction cost of -£6.79/t in its first, while system B has a high carbon reduction cost of £86.35/t.

(3) Further comparisons in different regions show that system-A has 89.42% to 132.87% higher annual *SPF* than system-B and achieves 1.88% to 21.53% reductions in annual heating bills and carbon emissions in non-extremely cold regions. Compared to system-C, system-A has 20.64% to 54.36% savings in annual heating bills and decreases the annual carbon emissions by 14.39% to 86.09% in regions with relatively low electricity prices.

(4) In extremely cold regions, system-A has obviously higher heating loads than system-B because of the unheated fresh air, resulting in 0.36% to 1.31% increases in annual heating bills and carbon emissions when compared to system-B. In regions with very high electricity prices, system-A has 28.29% to 66.56% increases in annual heating bills while reducing the annual carbon emissions by 4.99% to 88.21% compared to system-C. The application potential of system-A is, therefore, deeply analysed by comparing it to the conventional HP and gas boiler heating systems in wide regions with different weather conditions and regional energy policies, giving important guiding significance for the DSHP in the global application.

Acknowledgement

This work is funded by the UK BEIS project ‘A low carbon heating system for existing public buildings employing a highly innovative multiple-throughout-flowing micro-channel solar-panel-array and a novel mixed indoor/outdoor air source heat pump’ (LCHTIF1010) and International Exchange 2021 Cost Share (IEC\NSFC\211237). This work is also sponsored by the Chinese Scholarship Council.

References

[1] Global energy transformation-a roadmap to 2050. International renewable energy agency; 2019.

[2] Energy Security Bill factsheet: Low-carbon heat scheme. https://www.gov.uk/government/publications/energy-security-bill-factsheets/energy-security-bill-factsheet-low-carbon-heat-scheme: Department for Business, Energy & Industrial Strategy; 2022.

[3] Zhao H, Gao Y, Song Z. Strategic outlook of Heat pump development in China. 12th IEA Heat Pump Conference. 2017:1-5.

[4] REPowerEU: A plan to rapidly reduce dependence on Russian fossil fuels and fast forward the green transition. https://ec.europa.eu/commission/presscorner/detail/en/IP_22_3131: European Commission; 2022.

[5] Zhang Y, Ma Q, Li B, Fan X, Fu Z. Application of an air source heat pump (ASHP) for heating in Harbin, the coldest provincial capital of China. Energy Build. 2017;138:96-103.

[6] Song M, Deng S, Dang C, Mao N, Wang Z. Review on improvement for air source heat pump units during frosting and defrosting. Appl Energy. 2018;211:1150-70.

[7] Wang W, Ma Z, Jiang Y, Yang Y, Xu S, Yang Z. Field test investigation of a double-stage coupled heat pumps heating system for cold regions. International Journal of Refrigeration. 2005;28(5):672-9.

[8] Redón A, Navarro-Peris E, Pitarch M, González-Macia J, Corberán JM. Analysis and optimization of subcritical two-stage vapor injection heat pump systems. Appl Energy. 2014;124:231-40.

[9] Cheng Z, Wang B, Shi W, Li X. Performance evaluation of novel double internal auto-cascade two-stage compression system using refrigerant mixtures. Appl Therm Eng. 2020;168.

[10] Zou H, Li X, Tang M, Wu J, Tian C, Butrymowicz D, et al. Temperature stage matching and experimental investigation of high-temperature cascade heat pump with vapor injection. Energy. 2020;212.

[11] Han Z, Ju X, Qu L, Liu J, Ma X, Zhang S. Experimental study of the performance of a double-source heat-pipe composite vapour-compression heating unit. Sol Energy. 2017;155:1208-15.

[12] Wang Y, Quan Z, Jing H, Wang L, Zhao Y. Performance and operation strategy optimization of a new dual-source building energy supply system with heat pumps and energy storage. Energy Conv Manag. 2021;239.

[13] Jiang Y, Zhang H, Wang Y, Wang Y, Liu M, You S, et al. Research on the operation strategies of the solar assisted heat pump with triangular solar air collector. Energy. 2022;246.

[14] Grossi I, Dongellini M, Piazzi A, Morini GL. Dynamic modelling and energy performance analysis of an innovative dual-source heat pump system. Appl Therm Eng. 2018;142:745-59.

[15] Fang L, Wang Y. Exploring Application of Ice Source Heat Pump Technology in Solar Heating System for Space Heating. Energies. 2022;15(11).

[16] Li X, Lyu W, Ran S, Wang B, Wu W, Yang Z, et al. Combination principle of hybrid sources and three typical types of hybrid source heat pumps for year-round efficient operation. Energy. 2020;193.

[17] Kwak K, Bai C. A study on the performance enhancement of heat pump using electric heater under the frosting condition: Heat pump under frosting condition. Appl Therm Eng. 2010;30(6-7):539-43.

[18] Tan H, Xu G, Tao T, Sun X, Yao W. Experimental investigation on the defrosting performance of a finned-tube evaporator using intermittent ultrasonic vibration. Appl Energy. 2015;158:220-32.

[19] Park J-S, Kim DR, Lee K-S. Frosting behaviors and thermal performance of louvered fins with unequal louver pitch. International Journal of Heat and Mass Transfer. 2016;95:499-505.

[20] Zhong H, Zeng L, Long J, Xia K, Lu H, Yongga A. Anti-frosting operation and regulation technology of air-water dual-source heat pump evaporator. Energy. 2022;254.

[21] Wang F, Zhou Y, Yang W, Ni M, Zhang X, Liang C. Anti-frosting performance of sprayable superhydrophobic coating suitable for outdoor coil of air source heat pump. Appl Therm Eng. 2020;169.

[22] Dodoo A, Gustavsson L, Sathre R. Primary energy implications of ventilation heat recovery in residential buildings. Energy Build. 2011;43(7):1566-72.

[23] Fan Y, Li J, Zhao X, Myers S, Cheng Y, Yu M, et al. A proof-of-concept study of a novel ventilation heat recovery vapour injection air source heat pump. Energy Conv Manag. 2022;256.

[24] Ege A, Şahin HM. Uncertainties in energy and exergy efficiency of a High Pressure Turbine in a thermal power plant. International Journal of Hydrogen Energy. 2016;41(17):7197-205.

[25] ASHRAE. Ventilation for Acceptable Indoor Air Quality. 2019.

[26] Cui Y, Zhu Z, Zhao X, Li Z, Qin P. Bayesian Calibration for Office-Building Heating and Cooling Energy Prediction Model. Buildings. 2022;12(7).

[27] Flexi DV3600. https://www.airflow.com/product/duplexvent-flexi-range/90000070: AIRFLOW.

[28] Fitó J, Dimri N, Ramousse J. Improving Thermoeconomic and Environmental Performance of District Heating via Demand Pooling and Upscaling. Energies. 2021;14(24).

[29] Mahon C, Mediboyina MK, Gartland D, Murphy F. Life cycle assessment of Irish district heating systems: a comparison of waste heat pump, biomass-based and conventional gas boiler. Clean Technologies and Environmental Policy. 2022;24(5):1437-51.

[30] Reversible Air to Water Heat Pump Product Selection data. https://en.ahi-carrier.gr/product/30awh-reversible-air-to-water-heat-pump/: Carrier.

[31] Vocale P, Morini GL, Spiga M. Influence of Outdoor Air Conditions on the Air Source Heat Pumps Performance. Energy Procedia. 2014;45:653-62.

[32] CIBSE Top Tips Information Sheet 8: Temperature in Indoor Workplaces (Thermal Comfort). https://www.cibse.org/knowledge-research/knowledge-portal/ctt8-cibse-top-tips-8-temperature-in-indoor-workplaces-thermal-comfort: Chartered Institution of Building Services Engineers; 2015.

[33] Bionic. Business Gas & Electricity Tariff Prices per kWh. https://www.moneysupermarket.com/gas-and-electricity/business-energy/a/tariff-prices-per-kwh/.

[34] The Climate Transparency Report 2021. https://www.climate-transparency.org/g20-climate-performance/g20report2021#1531904804037-423d5c88-a7a7: Climate Transparency; 2021.

[35] Greenhouse gas reporting: conversion factors. https://www.gov.uk/government/publications/greenhouse-gas-reporting-conversion-factors-2021: Department for Business, Energy & Industrial Strategy; 2021.

[36] Greenhouse gas emission intensity of electricity generation in Europe. https://www.eea.europa.eu/ims/greenhouse-gas-emission-intensity-of-1: European Environment Agency; 2021.